PAPER

Check for updates

Electrospinning Cu–TiO$_2$ nanofibers used for photocatalytic disinfection of bacteriophage f2: preparation, optimization and characterization

Xiang Zheng,[a] Zhi-peng Shen,[a] Can Cheng,[a] Lei Shi,[a] Rong Cheng [iD] *[a] and Jing Dong[b]

The presence of pathogenic viruses in drinking water threatens public health severely. However, there is little information about how to use photocatalysts to disinfect viruses. In this report, one-dimensional Cu–TiO$_2$ nanofibers were fabricated using the electrospinning method and used for the removal of bacteriophage f2. The results showed that the optimum doping ratio and calcination temperature of the Cu–TiO$_2$ nanofibers was n(Cu) : n(Ti) = 1 : 8 and 450 °C, respectively. In addition, bacteriophage f2 with an initial concentration of 10^5 PFU mL^{-1} was completely inactivated with a dosage of 50 mg L^{-1} of Cu–TiO$_2$ nanofibers under visible light irradiation for 4 h. Furthermore, the results from characterization of the nanofibers by various techniques, including scanning electron microscopy (SEM), energy dispersive spectrometry (EDS), X-ray diffractometry (XRD), X-ray photoelectron spectroscopy (XPS) and UV-vis spectrophotometry demonstrated that TiO$_2$ existed in the anatase phase and Cu^{2+} substituted Ti^{4+} in the TiO$_2$ lattice. The introduction of Cu into TiO$_2$ effectively extended the spectral response of TiO$_2$ to visible light. On the basis of this evidence, the mechanism of virus inactivation by Cu–TiO$_2$ nanofibers was proposed.

Introduction

It is of great significance for human beings to have access to potable water. Ensuring water quality, especially microbiological quality, has been regarded as the top priority when supplying drinking water.[1] Pathogenic microorganisms in water, including bacteria, viruses, parasites, and so on, have received much attention for the microbial contamination they cause. Viruses are smaller in size and have stronger pathogenicity, posing a serious threat to public health after coming into contact with humans.[2] In the US, viruses led to a few outbreaks of waterborne diseases and they were more difficult to analyze than bacterial pathogens.[3] This calls for effective technologies to remove viruses from water.

Traditional disinfection methods can inactivate viruses to some extent, while there are also a series of problems. Chlorination is a dominant disinfection method, but it would produce disinfection by-products (DBPs), which are harmful to humans.[4–6] UV disinfection can avoid DBPs, but it requires comparatively more energy and the photoreactivation phenomenon occurs frequently.[7,8] Ozone is able to inactivate microorganisms in a short time owing to its strong oxidizing property, but it is unstable and has low solubility in water.[9,10] Membranes can control pathogenic bacteria and protozoa effectively; however, the outcome turns to be reversed for viruses because their sizes are far smaller than those of membrane pores.[11,12] In addition, the high cost and fouling of membrane are also limiting factors for its extensive application.

TiO$_2$ photocatalysis is a new advanced oxidation technology that rises rapidly in recent years. TiO$_2$ produces photoinduced electrons and holes after being excited by high-energy photons. The electrons and holes further react with the oxygen and hydroxyl group in water, then produce various reactive oxygen species (ROS) including ˙OH, ˙O$_2^-$, H$_2$O$_2$, ^{1}O$_2$. These ROS have strong oxidizability and are capable of degrading organic pollutants or inactivating microorganisms.[13–15] Over the last decades, TiO$_2$ photocatalysis has been widely studied and proved to be an effective, reliable disinfection method.[16] However, TiO$_2$ possesses large band gap, it can only be activated by UV and the utilization of the visible light is limited.[17] In addition, the photo-generated electrons/holes tend to recombine during the photocatalytic process, thus reducing the overall quantum efficiency.[18] For these problems, it has been well documented that metal doping is a promising method to extend the spectral response of TiO$_2$ to the visible light as well as decrease the electron–hole recombination rate.[19] Compared to other metal elements that are used as dopants, copper is relatively low-cost and widely used in daily life and industrial production, attracting many researchers' attention. Cu–TiO$_2$

School of Environment & Natural Resources, Renmin University of China, Beijing 100872, P. R. China. E-mail: chengrong@ruc.edu.cn; Tel: +86 1082502065

[b]Beijing Municipal Research Institute of Environmental Protection, Beijing, 100037, P. R. China

nanoparticles have been proved to show considerable photocatalytic performance in several literatures.[20,21] Nevertheless, the high aggregation tendency of nanoparticles significantly reduces the photocatalytic efficiency. One-dimensional (1D) nanofibers would be a better option due to their low aggregation tendency, high axial ratio, good mechanical properties and large surface areas, thus promoting the photocatalytic activity.[22] Electrospinning has been identified as the most advantageous method for nanofibers preparation owing to its simple operation, low cost and high efficiency.[23]

Most researchers prepared electrospinning Cu–TiO$_2$ nanofibers to produce hydrogen or degrade organic pollutants,[24–26] while very few pay attention to disinfection. Yousef *et al.* fabricated CuO/TiO$_2$ nanofibers *via* one-step electrospinning, and achieved high removal efficiency of pathogenic *Klebsiella pneumoniae* under visible light.[27] Despite that, no relevant research has been done for the disinfection of virus. There are differences between bacteria and viruses in structural and geometric properties.[28] Viruses are relatively smaller in size and have a strong resistance to traditional disinfection technologies, so the results of bacterial disinfection cannot be translated to viral disinfection, and it is significant to evaluate the antiviral performance of electrospinning Cu–TiO$_2$ nanofibers.

In this study, Cu–TiO$_2$ nanofibers were fabricated by electrospinning method. Several parameters including doping ratio, calcination temperature and fiber diameter were optimized. The optimized Cu–TiO$_2$ nanofibers were then characterized by scanning electron microscope (SEM), energy dispersive spectrometer (EDS), X-ray diffractometer (XRD), X-ray photoelectron spectroscopy (XPS) and UV-vis spectrophotometer. On basis of these characterizations, the disinfection mechanism of Cu–TiO$_2$ nanofibers was discussed in detail.

Experimental

Chemicals

Tetrabutyl titanate (TBOT), polyvinylpyrrolidone (PVP), cupric nitrate, anhydrous alcohol, acetic acid, hydrochloric acid, sodium hydroxide, nutrient agar medium, agar and nutrient broth. All chemicals were analytically pure and purchased from Sinopharm Chemical Reagent Beijing. The ultrapure water was obtained from a Milli Q system (Millipore, US).

Photocatalyst synthesis

3 g PVP was added into 45 mL anhydrous alcohol, and then the solution was stirred for several hours till it became uniform and transparent, which was marked as solution A. Certain amount of TBOT and cupric nitrate was successively added into the mixed solution of 20 mL anhydrous alcohol and 16 mL acetic acid, and then the solution was stirred for a certain time, which was marked as solution B. Finally, solution B was transferred into solution A slowly with stirring for about 1 h. Thus the precursor solution of electrospinning was successfully prepared.

The diagrammatic sketch of the electrospinning device was shown in Fig. 1. First, the synthetized precursor solution was
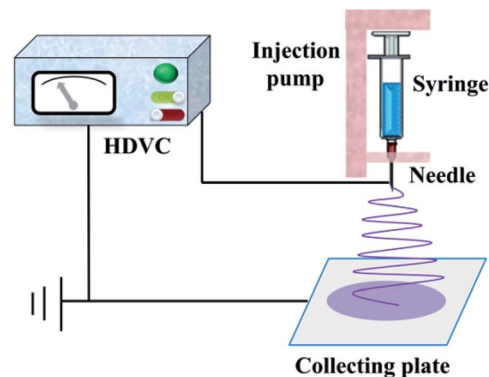

Fig. 1 Schematic diagram of the electrospinning device.

put into the syringe and then transferred to the injection pump. Second, the flow rate of injection pump and the operation voltage of high voltage DC power supply were adaptively adjusted, till the released liquid from the needle was sequentially stable and the jet trickle could be solidified into fibrous material before collected on the plate under the force of static electricity. After a period of time, the nanofiber mats were torn off from the collecting plate carefully and then calcined in a pipe electric furnace (SK-G10125K, ZhongHuan Electric Furnace Co. Ltd., China). The heating rate of the furnace was 2 °C min^{-1}, and the thermal retardation time was 2 h at the stated temperature.

Catalyst characterization

A JSM-6301F field emission scanning electron microscopy (SEM, JEOL Ltd., Japan) was applied to investigating the surface morphology of the as-obtained photocatalysts. The photocatalyst samples were coated with aurum before SEM analysis to enhance electrical conductivity. An energy dispersive X-ray spectroscopy (EDX) was applied to study the elemental composition of the photocatalysts. Crystalline structure of the photocatalysts was investigated by a X-ray diffractometer (XRD, Rigaku Co., Japan) with Cu Kα ($\lambda = 1.5418$ Å) radiation at an operating voltage of 40 kV, an emission current of 40 mA. The surface composition was detected *via* X-ray photoelectron spectroscopy analysis (XPS, Thermo Fisher Co., America) with the scan step of 0.05 eV per step. The optical properties of the photocatalysts were obtained using a UV-visible spectrophotometer (Varian Co., America).

Virus preparation and assay

Bacteriophage f2 and its host bacteria (*E. coli* 285) were bought from institute of Hygiene and Environmental Medicine, Academy of Military Medical Sciences, China. The duplication and purification process of bacteriophage f2 was followed by the method described in a previous research.[29] The concentration of bacteriophage f2 was determined by the double agar plate method. Petri dishes were put in the constant temperature incubator for 4 h at the temperature of 37 °C. Only the number of transparent plaques ranging from 30 to 300 on the plates was acceptable.
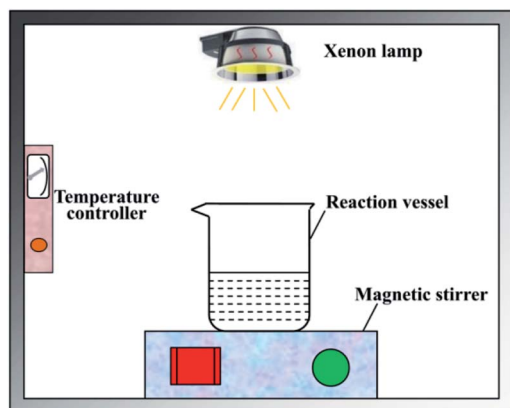
Fig. 2 Schematic diagram of the photocatalytic disinfection reactor.

Disinfection experiment

The disinfection experiment was carried out in a photocatalytic reactor which was shown in Fig. 2. The reaction vessel was a 500 mL beaker. First, 200 mL deionized water was added into the beaker after sterilization treatment. The pH value was adjusted to 7 by hydrochloric acid and sodium hydroxide solution. Second, the photocatalyst with a dose of 50 mg L^{-1} and concentrated liquid of bacteriophage f2 was put into the beaker successively, and the initial concentration of virus was 10^5 PFU mL^{-1}. Then the beaker was placed on a magnetic stirrer in order to keep the photocatalyst well separated in the reaction solution during the experiment. The visible light source was provided by a CEL-HXUV300 Xenon lamp (Beijing ZhongJiaoJinYuan Tech Co. Ltd., China) with a 400 nm cutoff filter, the visible light intensity was set as 100 mW cm^2. During the experiment, the whole system was kept closed in case of being interrupted by ambient light sources. The temperature of the reaction system was adjusted to 25 °C by a self-designed temperature controller, which consisted of a DLSB-2L/30 cryogenic coolant circulation pump (Gongyi YuHua Instrument Co. Ltd.) and a JRQM heater (Hunan HuaSi Instrument Co. Ltd.). Samples were taken from the beaker at certain time intervals. All the samples were treated for virus assay.

The photocatalytic disinfection efficiency of bacteriophage f2 was calculated with the equation:

$$Q = \log N_0 - \log N_t = -\log \frac{N_t}{N_0} \quad (1)$$

where Q represents the virus removal efficiency, t represents the reaction time, N_0 and N_t is the virus concentration at the initial time and time t, respectively.

Results and discussion

Optimization of Cu–TiO$_2$ nanofibers

Fig. 3 shows the virus removal efficiency of TiO$_2$ nanofibers doped with different contents of Cu. No significant virus removal was observed under visible light without any nanofibers, indicating that visible light didn't affect the activity of viruses. After adding pure TiO$_2$ nanofibers into the reaction
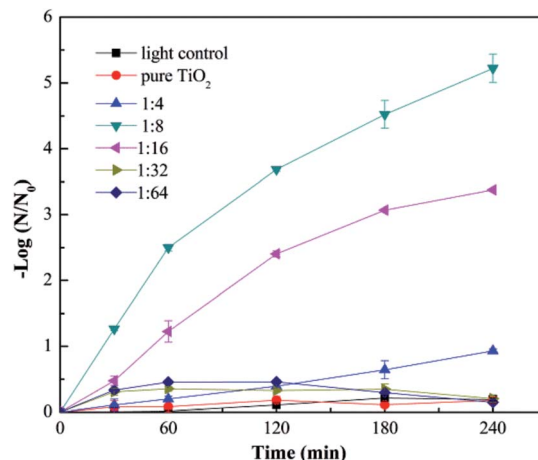

Fig. 3 Photocatalytic disinfection of bacteriophage f2 by Cu–TiO$_2$ with different mole ratios of Cu and Ti. Other conditions for nanofibers preparation: calcination temperature = 450 °C, TBOT dosage in precursor solution = 2 g.

system, there was still no obvious virus removal, suggesting that pure TiO$_2$ couldn't be activated by visible light. Then Cu-doped TiO$_2$ nanofibers with different mole ratio of Cu and Ti were investigated. Doping Cu into TiO$_2$ nanofibers significantly enhanced the virus removal efficiency. And the removal efficiency achieved the optimum when the mole ratio of Cu and Ti was 1 : 8. All viruses were inactivated after 4 h in this situation. This phenomenon confirmed that Cu modification successfully extended the spectral response of TiO$_2$ into the visible region. However, when the mole ratio of Cu and Ti increased to 1 : 4, the virus removal efficiency dropped dramatically. This trend was consistent with many other researchers.[30–32] Excessive content of Cu tended to cover the active sites on the TiO$_2$ surface as well as acting as the recombination centers for photogenerated electrons and holes, thus reducing the disinfection efficiency.[33,34]
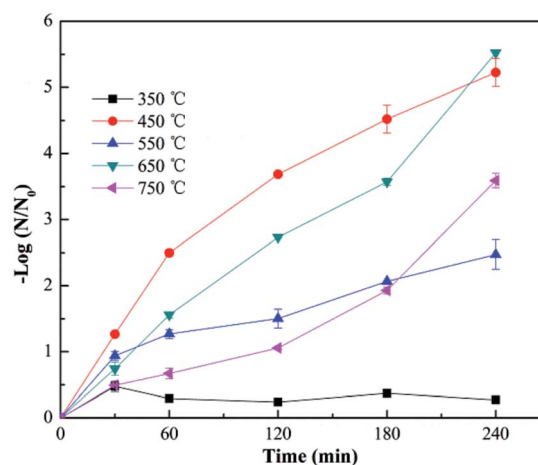

Fig. 4 Photocatalytic disinfection of bacteriophage f2 by Cu–TiO$_2$ treated at different calcination temperatures. Other conditions for nanofibers preparation: n(Cu) : n(Ti) = 1 : 8, TBOT dosage in precursor solution = 2 g.

Fig. 4 shows the virus removal efficiency of Cu–TiO$_2$ nanofibers treated at different calcination temperatures. No virus removal was achieved when the calcination temperature was 350 °C. As the temperature increased to 450 °C, all viruses were completely removed within 4 h. However, the removal efficiency decreased to some extent when the calcination temperature was over 450 °C. Calcination temperature could affect the crystal structure of TiO$_2$, thus influencing the photocatalytic activity.[35,36] Low removal efficiency at 350 °C might be due to the incomplete growth of crystals. As the temperature increased, TiO$_2$ is gradually transformed into anatase, and then rutile,[35] which was proved by the XRD test in Fig. 8. Normally, the anatase TiO$_2$ exhibits relative higher photocatalytic activity than rutile TiO$_2$, this could explain the optimum removal efficiency at 450 °C and lower removal efficiency at higher calcination temperatures. In addition, the nanocrystals tended to aggregate at over-high temperatures,[35] resulting in a negative effect on virus removal efficiency, which was also a reasonable explanation for the as-described phenomenon.

The effect of fiber diameter on virus removal efficiency was also investigated. The fiber diameter was adjusted by adjusting the addition amount of TBOT in the precursor solution, and the cupric nitrate dosage was adjusted correspondingly to maintain the mole ratios of Cu and Ti at 1 : 8. As shown in Fig. 5, the calcined Cu–TiO$_2$ nanofibers were characterized by SEM, and the diameter of the nanofibers was measured. The fiber diameter increased from 55 nm to 146 nm with the increase of TBOT dosage from 0.5 g to 4 g, then decreased to 81 nm as the TBOT dosage increased to 6 g. Generally, the fiber diameter would increase with the increase of TBOT dosage. However, to maintain the mole ratios of Cu and Ti at 1 : 8, the increase of TBOT dosage correspondingly increased the concentration of Cu^{2+} in the precursor solution, and appropriate addition of metal ions could increase the surface charge density of charged jet and speed up the movement of charges under the external electric field, which was conducive to the refinement of the jet, thus the fiber diameter became smaller.[37] The prepared Cu–TiO$_2$ nanofibers with different diameters were applied to the disinfection experiment. As shown in Fig. 6, fiber diameter exhibited no significant effect on virus removal efficiency, almost all the viruses were completely inactivated in 4 h. Li et al. prepared g-C$_3$N$_4$, N–TiO$_2$, Bi$_2$WO$_6$ and Ag@AgCl to inactivate MS2 under visible light,[38] although the experimental operating conditions were not exactly the same, it could be concluded that the as-prepared Cu–TiO$_2$ nanofibers showed better antiviral performance than N–TiO$_2$, Bi$_2$WO$_6$, and showed comparable performance with g-C$_3$N$_4$ and Ag@AgCl.

Characterization of Cu–TiO$_2$ nanofibers

The Cu–TiO$_2$ composite nanofibers were synthesized under the optimum condition (n(Cu) : n(Ti) = 1 : 8, calcination temperature = 450 °C, TBOT dosage in precursor solution = 2 g) for further characterization. In the first place, SEM was applied to investigating the morphology of the nanofibers. As shown in Fig. 7, after calcination, both of the diameters of TiO$_2$ and Cu–TiO$_2$ decreased from over 200 nm to about 140 nm, and all nanofibers maintained a good one dimensional structure. The thermal decomposition of PVP was responsible for the decrease of fiber diameters.[27] The melting point of PVP was about 150 °C, which was far below the calcination temperature (450 °C). In addition, it was observed that the surfaces of TiO$_2$ and Cu–TiO$_2$ nanofibers became rough after calcination, which might be caused by the crystallization of TiO$_2$.[39] The rough surfaces were reported to be conductive to improve photocatalytic activity.[26] It could also be observed that there were no significant differences in the morphology and diameter between TiO$_2$ and Cu–TiO$_2$ nanofibers. EDS spectrums of TiO$_2$ and Cu–TiO$_2$ nanofibers were shown in Fig. 7(e) and (f). The presence of Ti, O, Au and C elements were observed in TiO$_2$ nanofibers, and the mole ratio of O and Ti was 2.3 : 1, which was a possible evidence for the formation of TiO$_2$. Au element was derived from the application of gold film in the pre-treatment process of the samples. C
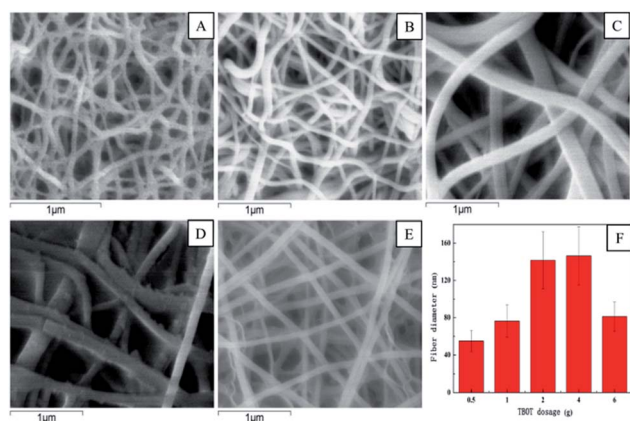

Fig. 5 SEM images of Cu–TiO$_2$ nanofibers with different TBOT dosage in precursor solution. (A) 0.5 g, (B) 1 g, (C) 2 g, (D) 4 g, (E) 6 g. (F) The determined fiber diameter of Cu–TiO$_2$ nanofibers with different TBOT dosage in precursor solution. Other conditions for nanofibers preparation: n(Cu) : n(Ti) = 1 : 8, calcination temperature = 450 °C.
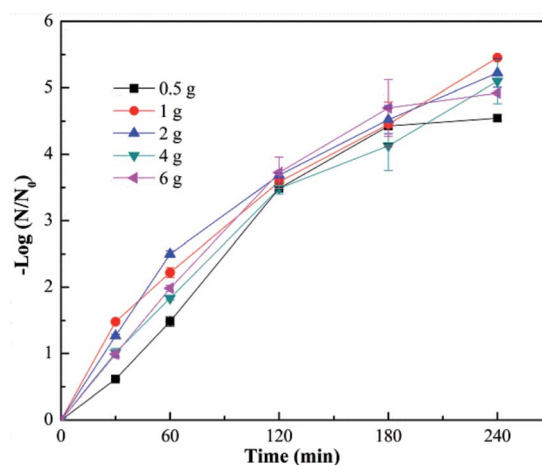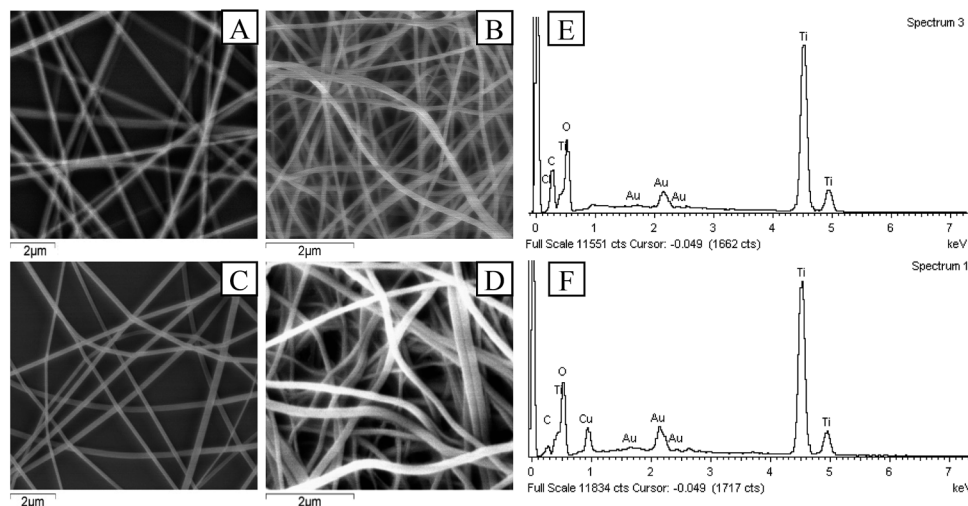

Fig. 6 Photocatalytic disinfection of bacteriophage f2 by Cu–TiO$_2$ with different TBOT dosage in precursor solution. Other conditions for nanofibers preparation: n(Cu) : n(Ti) = 1 : 8, calcination temperature = 450 °C.

Fig. 7 SEM images of (A) TiO_2 before calcination, (B) TiO_2 after calcination, (C) Cu–TiO_2 before calcination, (D) Cu–TiO_2 after calcination; EDS spectrums of (E) TiO_2 nanofibers and (F) Cu–TiO_2 nanofibers.

element was possibly due to the residue of PVP after calcination. In the EDS spectrum of Cu–TiO_2 nanofibers, Cu element was observed at 0.93 keV in addition to Ti, O, Au and C elements, and the mole ratio of Cu and Ti was around 1 : 7, which was close to the designed ratio (n(Cu) : n(Ti) = 1 : 8). It could be illustrated that Cu element was successfully introduced into TiO_2 nanofibers.

XRD spectrums were used to study the phase structures of TiO_2 and Cu–TiO_2 nanofibers. As shown in Fig. 8, for both of the nanofibers at the calcination temperature of 450 °C, the diffraction peaks at 2θ of 25.3°, 37.9°, 47.9°, 54.0°, 62.6°, 68.8°, 70.2°, 75.0°, 83.0° were correspond to the (101), (103), (200), (105), (213), (116), (220), (107), (303) crystal planes of the anatase TiO_2 phase. The rutile TiO_2 phase was not presented. Compared to pure TiO_2, the diffraction peaks of Cu–TiO_2 at 450 °C were enhanced, indicating that doping Cu into TiO_2 promoted the formation of anatase TiO_2. The diffraction peaks of Cu or Cu oxides in Cu–TiO_2 were not observed at 450 °C,

which was consistent with the research conducted by Lin et al.[40] The possible reason may be that Cu is highly dispersed within TiO_2 crystal lattice or that the content of Cu or Cu oxides is below the detection limit of XRD. However, the diffraction peaks of CuO were observed at 650 °C, ruling out the latter possibility. Therefore, it could be inferred that Cu was successfully doped into the crystal lattice of TiO_2 at 450 °C.[41] In addition, a slight shift in the peaks of Cu–TiO_2 calcined at 450 °C compared to pure TiO_2 was observed, which was also an evidence of the incorporation of Cu ions into the TiO_2 lattice.[41]

The chemical states of the elements in the calcinated nanofibers were determined by XPS analysis. C 1s peak at binding energy of 284.6 eV was applied as the reference for calibration. The XPS survey spectrum shown in Fig. 9(b) confirmed the introduction of Cu element in Cu–TiO_2 nanofibers compared to pure TiO_2 nanofibers (Fig. 9(a)), which was in accordance with the results of EDS. High resolution XPS spectrums for Cu 2p, Ti 2p and O 1s of Cu–TiO_2 nanofibers were shown in Fig. 9(c)–(e). The peaks at binding energy of 934.92 eV and 954.92 eV were respectively correspond to Cu $2p_{3/2}$ and Cu $2p_{1/2}$ (Fig. 9(c)), indicating that Cu existed as Cu^{2+} in Cu–TiO_2 nanofibers.[31] The shakeup satellite peaks at 944.22 eV and 963.17 eV ruled out the existence of Cu^+, further demonstrating that the only oxidation state of Cu is +2. The peaks around binding energy of 458.57 eV and 464.27 eV represented Ti $2p_{3/2}$ and Ti $2p_{1/2}$ respectively (Fig. 9(d)), which was correspond to the tetragonal crystal structure of Ti^{4+}. Meanwhile, the asymmetry of O 1s spectrum illustrated that at least two kinds of binding state of oxygen were existed in Cu–TiO_2 nanofibers (Fig. 9(e)). The peak at 529.97 eV was associated with the lattice oxygen in Cu–TiO_2 nanofibers.[42] The peak at higher binding energy of 531.7 eV was indicative of surface contamination by hydroxides from the atmosphere.[43] According to the results of XRD and XPS, it could be inferred that Cu^{2+} penetrated into the TiO_2 lattice and substituted the Ti^{4+}, forming new Cu–O–Ti bonds in Cu–TiO_2 nanofibers.
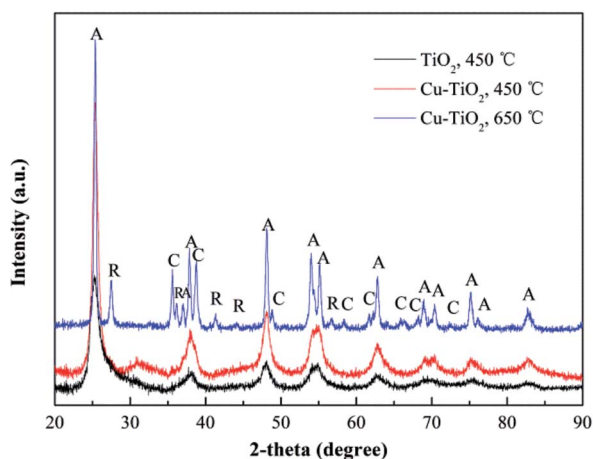

Fig. 8 XRD patterns of TiO_2 and Cu–TiO_2 nanofibers. n(Cu) : n(Ti) = 1 : 8. A: anatase, R: rutile, C: CuO.
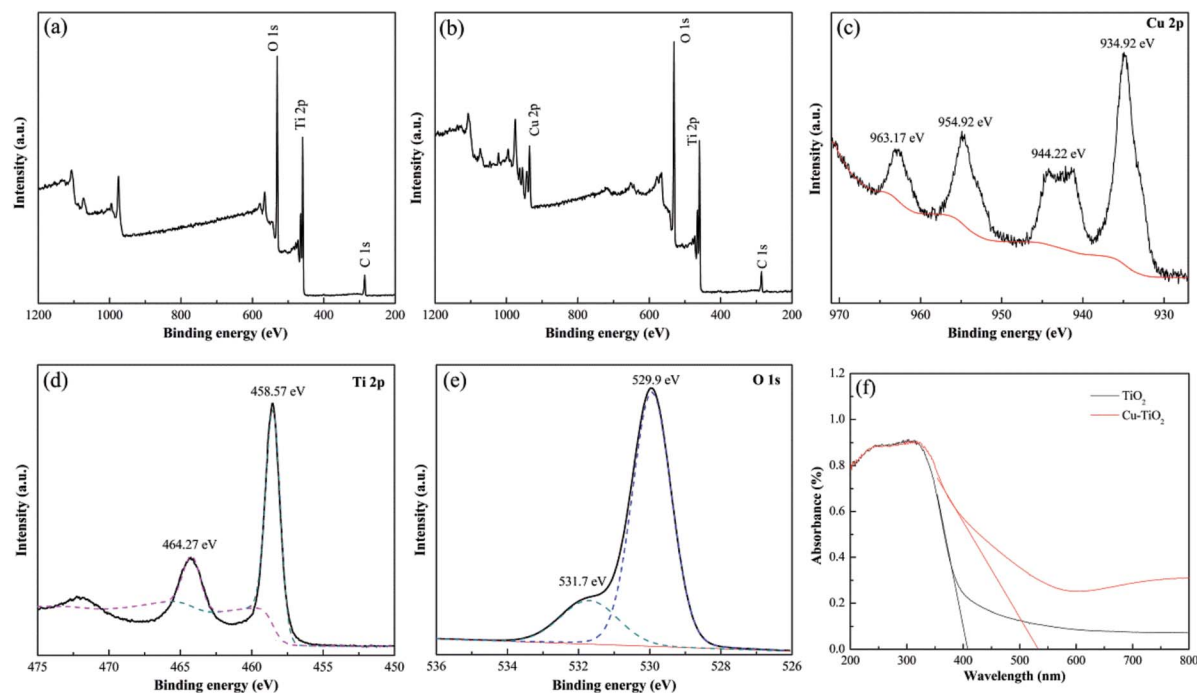
Fig. 9 XPS survey spectrums for (a) TiO_2 nanofibers and (b) $Cu–TiO_2$ nanofibers; high resolution XPS spectrums of $Cu–TiO_2$ nanofibers for (c) Cu 2p, (d) Ti 2p, (e) O 1s; (f) UV-vis absorption spectrums of TiO_2 and $Cu–TiO_2$ nanofibers.

The UV-vis absorption spectrums of TiO_2 and $Cu–TiO_2$ nanofibers were displayed in Fig. 9(f). For pure TiO_2 nanofibers, characteristic peak attributed to adsorption of UV irradiation were obvious from 200 to 400 nm. However, there was no absorption peak at 400–800 nm, indicating that pure TiO_2 cannot absorb visible light irradiation. For $Cu–TiO_2$ nanofibers, the absorption intensity of UV irradiation was increased compared to pure TiO_2 nanofibers, indicating that doping Cu into TiO_2 improved the utilization ratio of UV irradiation. In addition, the characteristic peak of $Cu–TiO_2$ was obviously extended to the visible light region, resulting in the red shift of absorption spectrum. It was calculated by Kubelkae–Munk function that the band gaps of pure TiO_2 and $Cu–TiO_2$ nanofibers were 3.01 eV and 2.30 eV respectively. This illustrated that $Cu–TiO_2$ nanofibers were promising photocatalysts under visible light.

successfully narrowed the bind gap of $Cu–TiO_2$ nanofibers to 2.30 eV (Fig. 9(f)), which could be activated by visible light. According to the XRD and XPS results, the doped Cu^{2+} substituted Ti^{4+} in the crystal lattice of TiO_2. This resulted in the formation of an impurity energy level below the conduction band of TiO_2.[14] As shown in Fig. 10, under visible light irradiation, the electrons in TiO_2 were excited from its valence band (VB) to the impurity energy level first and then transferred to the conduction band (CB). Part of the electrons in CB would transfer back to the impurity energy level due to potential difference while the others took part in the reaction with surface adsorbed O_2 to produce $^\cdot O_2^-$ (eqn (3)). Subsequently, $^\cdot O_2^-$ underwent facile disproportionation to produce $^\cdot OH$, H_2O_2 and $^1O_2$ (eqn (4)–(6)).[44] The separated holes in the VB of TiO_2 were positive enough to oxidize H_2O/OH^- into $^\cdot OH$ (eqn (7) and (8))
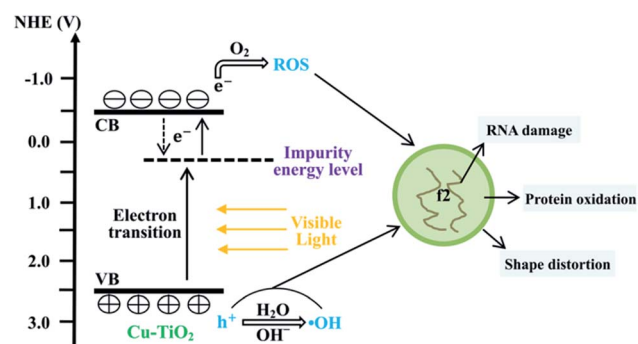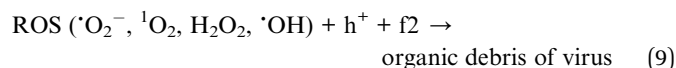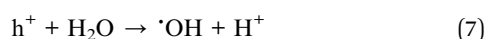
Mechanism of virus inactivation by $Cu–TiO_2$ nanofibers

The first step of the virus inactivation process is the adsorption of bacteriophage f2 onto the surfaces of $Cu–TiO_2$ nanofibers. The SEM images (Fig. 7) showed that the $Cu–TiO_2$ nanofibers maintained a good one dimensional structure and their surfaces became rough after calcination, which was conductive to the adsorption process, ensuring desirable disinfection efficiency consequently. Pure TiO_2 nanofibers were not able to inactivate bacteriophage f2 under visible light (Fig. 3), since its bind gap was up to 3.01 eV as we calculated (Fig. 9(f)), which was too high to be excited by visible light. Optimized $Cu–TiO_2$ nanofibers achieved 100% inactivation of bacteriophage f2 in 4 h under visible light, since the introduction of Cu^{2+}
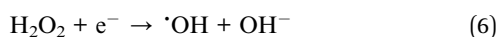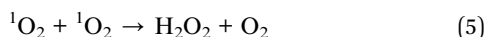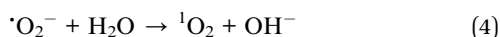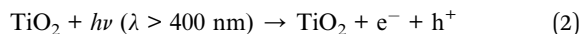

Fig. 10 Sketch map of proposed mechanism for viral inactivation by $Cu–TiO_2$ nanofibers under visible light irradiation.

as well as attack and oxidize the viruses directly.[45] Generally, holes and ROS generated from electrons and holes contributed to the inactivation of bacteriophage f2 collectively (eqn (9)). Furthermore, the oxidative holes and ROS tended to distort the viral particle shapes and damage the surface proteins primarily, and then destroy the major types of RNA genes, resulting in definite viral death.[38]

$$TiO_2 + h\nu\ (\lambda > 400\ nm) \rightarrow TiO_2 + e^- + h^+ \qquad (2)$$

$$O_2 + e^- \rightarrow {}^{\cdot}O_2^- \qquad (3)$$

$${}^{\cdot}O_2^- + H_2O \rightarrow {}^1O_2 + OH^- \qquad (4)$$

$${}^1O_2 + {}^1O_2 \rightarrow H_2O_2 + O_2 \qquad (5)$$

$$H_2O_2 + e^- \rightarrow {}^{\cdot}OH + OH^- \qquad (6)$$

$$h^+ + H_2O \rightarrow {}^{\cdot}OH + H^+ \qquad (7)$$

$$h^+ + OH^- \rightarrow {}^{\cdot}OH \qquad (8)$$

$$ROS\ ({}^{\cdot}O_2^-,\ {}^1O_2,\ H_2O_2,\ {}^{\cdot}OH) + h^+ + f2 \rightarrow$$
$$organic\ debris\ of\ virus \qquad (9)$$

Conclusions

Cu–TiO₂ nanofibers were prepared with electrospinning method and exhibited excellent antiviral performance under visible light. The optimum doping ratio and calcination temperature were $n(Cu) : n(Ti) = 1 : 8$ and 450 °C respectively. Cu–TiO₂ nanofibers with various diameters (55–146 nm) didn't show obvious differences in virus removal efficiency. Characterization of Cu–TiO₂ nanofibers demonstrated that Cu^{2+} substituted Ti^{4+} in the TiO₂ lattice and formed an impurity energy level below the conduction band of TiO₂, which enabled the nanofibers to realize visible light response. This study provides a promising technology for viral disinfection in drinking water.

Conflicts of interest

There are no conflicts to declare.

Acknowledgements

Notes and references

1 M. Khraisheh, L. Wu, A. H. Ala and M. A. Al-Ghouti, *J. Ind. Eng. Chem.*, 2015, **28**, 369–376.

2 S. Pedley and K. Pond, *Emerging issues in water and infectious disease*, World Health Organization, 2003.

3 J. L. Liang, E. J. Dziuban, G. F. Craun, V. Hill, M. R. Moore, R. J. Gelting, R. L. Calderon, M. J. Beach and S. L. Roy, *MMWR Surveillance Summaries*, 2006, **55**, 31–65.

4 S. E. Hrudey, *Water Res.*, 2009, **43**, 2057–2092.

5 R. Sadiq and M. J. Rodriguez, *Sci. Total Environ.*, 2004, **321**, 21–46.

6 J. Sohn, G. Amy, J. Cho, Y. Lee and Y. Yoon, *Water Res.*, 2004, **38**, 2461–2478.

7 R. A. Rodriguez, S. Bounty, S. Beck, C. Chan, C. McGuire and K. G. Linden, *Water Res.*, 2014, **55**, 143–149.

8 M. Guo, J. Huang, H. Hu, W. Liu and J. Yang, *Water Res.*, 2012, **46**, 4031–4036.

9 G. Shin and M. D. Sobsey, *Appl. Environ. Microbiol.*, 2003, **69**, 3975–3978.

10 V. Lazarova, P. Liechti, P. Savoye and R. Hausler, *J. Water Reuse Desalin.*, 2013, **3**, 337–345.

11 J. G. Jacangelo, S. S. Adham and J. Laîné, *J. - Am. Water Works Assoc.*, 1995, **87**, 107–121.

12 S. S. Madaeni, A. G. Fane and G. S. Grohmann, *J. Membr. Sci.*, 1995, **102**, 65–75.

13 W. Wang, G. Huang, C. Y. Jimmy and P. K. Wong, *J. Environ. Sci.*, 2015, **34**, 232–247.

14 S. Malato, P. Fernández-Ibáñez, M. I. Maldonado, J. Blanco and W. Gernjak, *Catal. Today*, 2009, **147**, 1–59.

15 M. N. Chong, B. Jin, C. W. Chow and C. Saint, *Water Res.*, 2010, **44**, 2997–3027.

16 C. McCullagh, J. M. Robertson, D. W. Bahnemann and P. K. Robertson, *Res. Chem. Intermed.*, 2007, **33**, 359–375.

17 S. G. Kumar and L. G. Devi, *J. Phys. Chem. A*, 2011, **115**, 13211–13241.

18 W. Choi, A. Termin and M. R. Hoffmann, *J. Phys. Chem.*, 1994, **98**, 13669–13679.

19 M. Pelaez, N. T. Nolan, S. C. Pillai, M. K. Seery, P. Falaras, A. G. Kontos, P. S. Dunlop, J. W. Hamilton, J. A. Byrne and K. O'Shea, *Appl. Catal., B*, 2012, **125**, 331–349.

20 C. Karunakaran, G. Abiramasundari, P. Gomathisankar, G. Manikandan and V. Anandi, *J. Colloid Interface Sci.*, 2010, **352**, 68–74.

21 B. Wu, R. Huang, M. Sahu, X. Feng, P. Biswas and Y. J. Tang, *Sci. Total Environ.*, 2010, **408**, 1755–1758.

22 S. K. Choi, S. Kim, S. K. Lim and H. Park, *J. Phys. Chem. C*, 2010, **114**, 16475–16480.

23 D. Li, J. T. McCann, Y. Xia and M. Marquez, *J. Am. Ceram. Soc.*, 2006, **89**, 1861–1869.

24 A. Yousef, N. A. Barakat and H. Y. Kim, *Appl. Catal., A*, 2013, **467**, 98–106.

25 S. S. Lee, H. Bai, Z. Liu and D. D. Sun, *Water Res.*, 2013, **47**, 4059–4073.

26 S. S. Lee, H. Bai, Z. Liu and D. D. Sun, *Appl. Catal., B*, 2013, **140**, 68–81.

27 A. Yousef, N. A. Barakat, T. Amna, S. S. Al-Deyab, M. S. Hassan, A. Abdel-hay and H. Y. Kim, *Ceram. Int.*, 2012, **6**, 4525–4532.

28 F. Chen, X. Yang, H. K. Mak and D. W. Chan, *Build Environ.*, 2010, **45**, 1747–1754.

29 R. Cheng, G. Li, C. Cheng, P. Liu, L. Shi, Z. Ma and X. Zheng, *Chem. Eng. J.*, 2014, **252**, 150–158.

30 S. Qin, F. Xin, Y. Liu, X. Yin and W. Ma, *J. Colloid Interface Sci.*, 2011, **356**, 257–261.

31 T. Pham and B. Lee, *Appl. Surf. Sci.*, 2014, **296**, 15–23.

32 W. Chen, V. Jovic, D. Sun-Waterhouse, H. Idriss and G. I. Waterhouse, *Int. J. Hydrogen Energy*, 2013, **38**, 15036–15048.

33 J. Wu, C. Li, X. Zhao, Q. Wu, X. Qi, X. Chen, T. Hu and Y. Cao, *Appl. Catal., B*, 2015, **176**, 559–569.

34 P. Khemthong, P. Photai and N. Grisdanurak, *Int. J. Hydrogen Energy*, 2013, **38**, 15992–16001.

35 J. Yu, H. Yu, B. Cheng and C. Trapalis, *J. Mol. Catal. A: Chem.*, 2006, **249**, 135–142.

36 D. J. Kim, S. H. Hahn, S. H. Oh and E. J. Kim, *Mater. Lett.*, 2002, **57**, 355–360.

37 X. Zong, K. Kim, D. Fang, S. Ran, B. S. Hsiao and B. Chu, *Polymer*, 2002, **43**, 4403–4412.

38 Y. Li, C. Zhang, D. Shuai, S. Naraginti, D. Wang and W. Zhang, *Water Res.*, 2016, **106**, 249–258.

39 J. Lee, S. Divya, P. Shanmugasundaram and P. I. Gouma, *J. Nanoeng. Nanomanuf.*, 2014, **4**, 140–145.

40 C. Lin and W. Yang, *Chem. Eng. J.*, 2014, **237**, 131–137.

41 X. Yang, W. Shu, H. Sun, X. Wang and J. Lian, *Trans. Nonferrous Met. Soc. China*, 2015, **25**, 504–509.

42 L. Zhu, M. Hong and G. W. Ho, *Nano Energy*, 2015, **11**, 28–37.

43 S. Xu, A. J. Du, J. Liu, J. Ng and D. D. Sun, *Int. J. Hydrogen Energy*, 2011, **36**, 6560–6568.

44 C. A. Castro, P. Osorio, A. Sienkiewicz, C. Pulgarin, A. Centeno and S. A. Giraldo, *J. Hazard. Mater.*, 2012, **211**, 172–181.

45 D. Xia, T. An, G. Li, W. Wang, H. Zhao and P. K. Wong, *Water Res.*, 2016, **99**, 149–161.